BIOCHEMISTRY
including biophysical chemistry & molecular biology

Article

pubs.acs.org/biochemistry

Nuclear Magnetic Resonance Structure of the Cytoplasmic Tail of Heparin Binding EGF-like Growth Factor (proHB-EGF-CT) Complexed with the Ubiquitin Homology Domain of Bcl-2-Associated Athanogene 1 from *Mus musculus* (mBAG-1-UBH)

Kuo-Wei Hung,*[,†] Hsiao-Wen Huang,[‡] Ching-Chang Cho,[‡] Sheng-Chieh Chang,[‡] and Chin Yu*[,‡]

[†]Instrumentation Center, National Tsing Hua University, Hsinchu 30013, Taiwan

[‡]Department of Chemistry, National Tsing Hua University, Hsinchu 30013, Taiwan

ABSTRACT: The membrane form of heparin binding EGF-like growth factor (proHB-EGF) yields secreted HB-EGF and a membrane-anchored cytoplasmic tail (proHB-EGF-CT), which may be targeted to the nuclear membrane after a shedding stimulus. Bcl-2-associated athanogene 1 (BAG-1) accumulates in the nuclei and inhibits apoptosis in adenoma-derived cell lines. The maintenance of high levels of nuclear BAG-1 enhances cell survival. However, the ubiquitin homology domain of BAG-1 from *Mus musculus* (mBAG-1-UBH) is proposed to interact with proHB-EGF-CT, and this interaction may enhance the cytoprotection against the apoptosis inducer. The mechanism of the synergistic anti-apoptosis function of proHB-EGF-CT and mBAG-1-UBH is still unknown. We offer a hypothesis that proHB-EGF-CT can maintain high levels of nuclear BAG-1. In this study, we first report the three-dimensional nuclear magnetic resonance structure of proHB-EGF-CT complexed with mBAG-1-UBH. In the structure of the complex, the residues in the C-terminus and one turn between β-strands β1 and β2 of mBAG-1-UBH bind to two terminals of proHB-EGF-CT, which folds into a loop with end-to-end contact. This end-to-end folding of proHB-EGF-CT causes the basic amino acids to colocalize and form a positively charged groove. The dominant forces in the binding interface between proHB-EGF-CT and mBAG-1-UBH are charge−charge interactions. On the basis of our mutagenesis results, the basic amino acid cluster in the N-terminus of proHB-EGF-CT is the crucial binding site for mBAG-1-UBH, whereas another basic amino acid in the C-terminus facilitates this interaction. Interestingly, the mBAG-1-UBH binding region on the proHB-EGF-CT peptide is also involved in the region found to be important for nuclear envelope targeting, supporting the hypothesis that proHB-EGF-CT is most likely able to trigger the nuclear translocation of BAG-1 in keeping its level high.

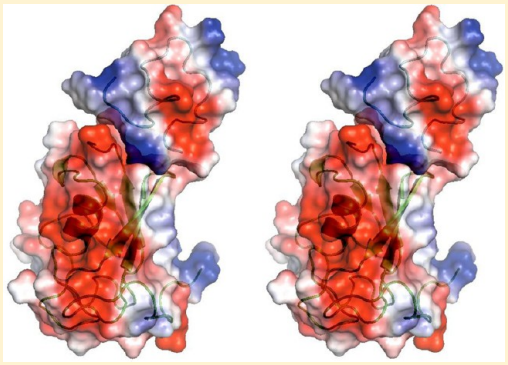

The precursor of heparin binding EGF-like growth factor (proHB-EGF) is synthesized as a membrane-anchored protein, which contains an extracellular domain, a transmembrane segment, and a short cytoplasmic tail.[1] After a shedding stimulus, the soluble HB-EGF is released from the cell surface and the membrane-anchored C-terminal domain of proHB-EGF (proHB-EGF-C) becomes internalized and targets the nucleus.[2] Ectodomain shedding can be triggered by a variety of stimuli, such as 12-*O*-tetradecanoyl phorbol 13-acetate (TPA),[3] calcium ionophores,[4] cellular stress and inflammation,[5] and apoptosis.[6,7] The nuclear translocation of proHB-EGF-C is found to induce cancer cell invasion and cell proliferation.[8,9] The 24-amino acid tail domain (proHB-EGF-CT, residues 185−208) downstream from the transmembrane domain is composed of three characteristic clusters of charged amino acid residues (Figure 1A,B).[10] Precursors of other EGF family members also possess similar charged amino acid clusters in their cytoplasmic domains (Figure 1B). Several functional proHB-EGF-CT interactors have been reported, such as the cochaperone Bcl-2-associated athanogene 1 (BAG-1)[11] and the transcriptional repressors promyelocytic leukemia zinc finger protein (PLZF) and B cell lymphoma 6 (Bcl6), resulting in the inhibition of PLZF- and Bcl6-mediated gene repression.[9,12,13]

Unlike nuclear protein PLZF and Bcl6, BAG-1 is generated as multiple isoforms that have distinct localizations within the cell. There are three isoforms of human BAG-1. BAG-1L is located in the nucleus, and BAG-1M and BAG-1S are located in both the nucleus and the cytoplasm. Only two isoforms, BAG-1L and BAG-1S, are observed in mouse BAG-1.[14] Mouse BAG-1S (219 amino acids) has been reported to be a proHB-EGF-CT binding partner based on yeast two-hybrid screening. The ubiquitin homology domain of mBAG-1 (mBAG-1-UBH, residues 1−97) is responsible for proHB-EGF-CT binding. The presence of mBAG-1 and proHB-EGF in CHO cells demonstrates the increased resistance to apoptosis induced by etoposide, in comparison to cells expressing either mBAG-1 or

Received: August 19, 2013
Published: March 14, 2014

dx.doi.org/10.1021/bi5003019 | *Biochemistry* 2014, 53, 1935−1946

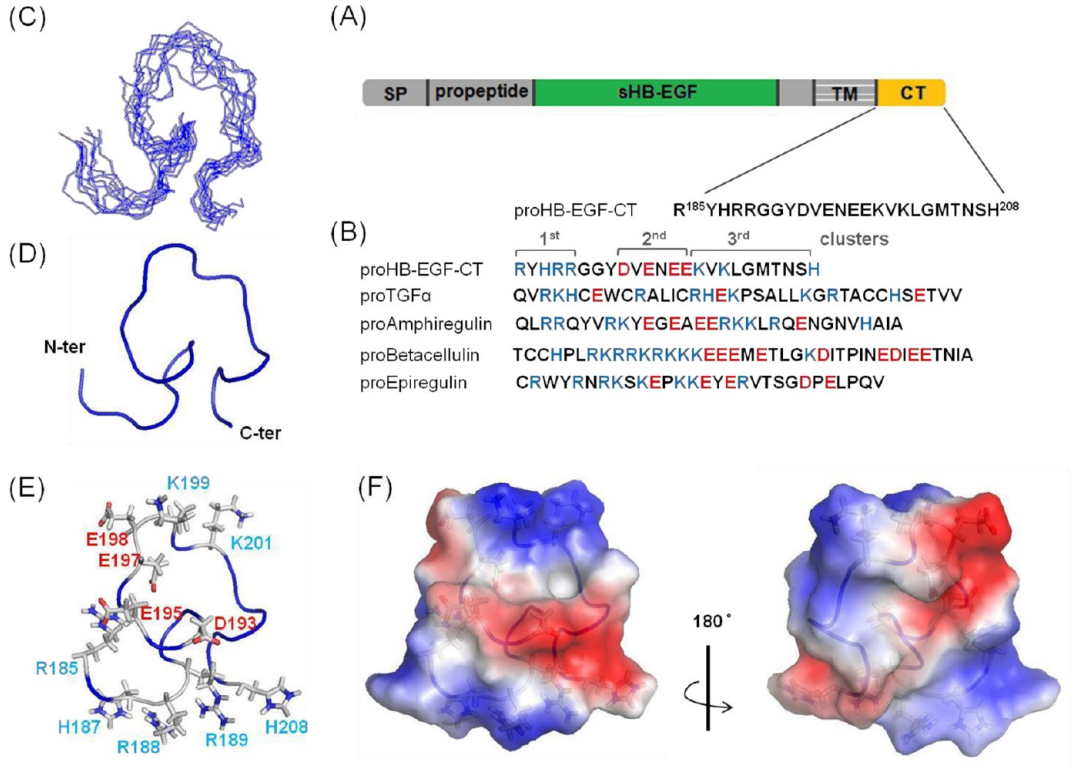

Figure 1. Amino acid sequence and solution structure of proHB-EGF-CT in the mBAG-1-UBH-bound form. (A) Schematic structure of the HB-EGF precursor. HB-EGF is synthesized and expressed at the plasma membrane as proHB-EGF. The cleavage at the juxtamembrane domain yields a soluble HB-EGF (sHB-EGF) and a C-terminal fragment containing the transmembrane domain (TM) and cytoplasmic tail domain (CT, amino acids 185−208). SP is the signal peptide. (B) Three characteristic clusters of charged amino acid residues within proHB-EGF-CT. The first is a positively charged cluster (RYHRR, colored blue), the second a negatively charged cluster (DVENEE, colored red), and the third a positively charged cluster (KKH, colored blue). The cytoplasmic domains of the other four EGF family precursors are listed below with the positively charged residues labeled in blue and the negatively charged residues labeled in red. (C) Superposition of the backbone atoms of the 10 final solution structures of proHB-EGF-CT in complex form and (D) the ribbon representation of the average structure. (E) Mapping of the basic (blue) and acidic (red) residues onto the average structure of proHB-EGF-CT. (F) Views (180°) of proHB-EGF-CT with semitransparent electrostatic potential surfaces.

proHB-EGF alone.[11] The mechanism causing the synergistic effect of BAG-1 and proHB-EGF on anti-apoptosis function is still unknown. Another report shows that nuclear BAG-1 inhibits apoptosis in a colorectal adenoma-derived cell line. A decrease in the level of nuclear expression and an increase in the level of cytoplasmic BAG-1 expression were observed in the cells treated with certain apoptosis inducers. BAG-1S, which is preferentially located in the cytoplasm, is fused with a nuclear localization signal (NLS) that protects against γ-radiation-induced apoptosis.[15] These results suggest that proHB-EGF-CT is most likely able to trigger the nuclear translocation of BAG-1. Interestingly, it has been shown that insertion of the proHB-EGF-CT peptide results in the targeting of a membrane protein to the nucleus. The crucial amino acids in proHB-EGF-CT for nuclear localization are identified as residues 185−198, a sequence motif distinct from the classical NLS.[16] On the other hand, the nuclear export of PLZF is also mediated by the interactions with the charged amino acids within the range of residues 185−198 of proHB-EGF-CT.[10] These results indicate that the cytoplasmic tail domain of proHB-EGF is a multifunctional domain that contains sorting signals involved in protein trafficking, and these signals are likely to be regulated by protein modification. Further studies will be necessary to determine the exact protein modifications and conformation of this peptide.

In this study, we first report the structure of the 24-amino acid peptide proHB-EGF-CT in bound form and identify the binding interface residues for the determination of the structure of the proHB-EGF-CT/mBAG-1-UBH binary complex using nuclear magnetic resonance (NMR) spectroscopy. In addition, the previously reported residues crucial for nuclear import or export were also mapped onto the solution structure of proHB-EGF-CT. Our findings provide valuable structural insight for understanding the multifunctionality of proHB-EGF-CT.

MATERIALS AND METHODS

Expression and Purification of the Protein and Peptide. The mBAG-1-UBH protein (residues 1−97) and the proHB-EGF-CT peptide (residues 185−208) were expressed and purified as described previously.[17] proHB-EGF-CT with the R188E point-mutat and the form truncated at His[208] were also expressed and purified using the same protocol. The ^{2}H-labeled sample was achieved by growing the *Escherichia coli* cells in M9 minimal medium supplemented with [^{12}C,^{1}H]-D-glucose in D_2O.

NMR Spectroscopy. The complete resonance assignments and three-dimensional structure determination of mBAG-1-UBH based on NMR spectroscopy have been reported previously.[17,18] The NMR structure of proHB-EGF-CT complexed with mBAG-1-UBH is calculated in this study. Various multidimensional NMR experiments used for the

dx.doi.org/10.1021/bi5003019 | *Biochemistry* 2014, 53, 1935−1946

resonance assignments of proHB-EGF-CT complexed with mBAG-1-UBH were conducted at 25 °C on a VARIAN 700 MHz NMR spectrometer equipped with a cryogenic probe. The mixture of ^{15}N- and ^{13}C-labeled proHB-EGF-CT (2 mM) and unlabeled mBAG-1-UBH (2 mM) was prepared in NMR buffer [20 mM phosphate-buffered saline (PBS) buffer (pH 6.0), 100 mM NaCl, and 5 mM DTT] supplemented with 10% D_2O to a final sample volume of approximately 500 μL. The sample for two-dimensional ^{1}H−^{1}H NOESY was prepared with equimolar concentrations of 1.0 mM of both unlabeled proHB-EGF-CT and ^{2}H-labeled mBAG-1-UBH in the same NMR buffer. The sequential assignment for the backbone resonance was performed using triple-resonance HNCA[19] and HN(CO)-CA.[20] The carbonyl carbon chemical shifts were determined using data from the HNCO experiment.[21] The side chain proton and carbon spin systems were determined using the CC(CO)NH,[22] HC(CO)NH,[22] HBHA(CO)NH,[23] and HCCH-TOCSY experiments.[24] The intramolecular nuclear Overhauser effects (NOEs) were obtained from ^{15}N-edited NOESY-HSQC, ^{13}C-edited NOESY-HSQC,[25] and two-dimensional (2D) ^{1}H−^{1}H NOESY[26] experiments; the intermolecular NOEs between unlabeled proHB-EGF-CT and ^{15}N- and ^{13}C-labeled mBAG-1-UBH were obtained from ^{13}C F1-filtered, F3-edited NOESY-HSQC spectra.[27] All the NOESY spectra were recorded with a mixing time of 150 ms for the determination of the structure of proHB-EGF-CT in complex form. All NMR data were processed and analyzed using VNMRJ and SPARKY, respectively.[28]

Chemical Shift Perturbation Measurement. The molecular characteristics of proHB-EGF-CT binding with mBAG-1-UBH were studied using ^{15}N−^{1}H HSQC spectra recorded at 25 °C. Residues involved in binding sites were mapped by analyzing the chemical shift perturbations (CSPs). The ^{15}N−^{1}H HSQC spectrum of free ^{15}N-labeled proHB-EGF-CT (1 mM) was first recorded and then the sample titrated with an increasing amount of unlabeled mBAG-1-UBH. The observed CSPs were weighted according to $(0.04\delta_N^2 + \delta_H^2)^{0.5}$, where δ_N and δ_H represent the change in nitrogen and proton chemical shifts, respectively.[29]

^{15}N NMR Relaxation Measurement. The ^{15}N-labeled proHB-EGF-CT samples in the absence and presence of unlabeled mBAG-1-UBH at a 1:1 molar ratio were prepared for the NMR measurements of longitudinal relaxation rate R_1, transverse relaxation rate R_2, and ^{1}H−^{15}N steady-state heteronuclear NOEs at 25 °C. The R_1 and R_2 spectra were recorded at 700 MHz with relaxation delays ranging from 10 to 1400 ms and from 10 to 250 ms, respectively. The ^{1}H−^{15}N heteronuclear NOEs were obtained by acquiring spectra at 700 MHz without and with a 3 s proton presaturation.

Isothermal Titration Calorimetry (ITC). The binding affinity between mBAG-1-UBH and wild-type proHB-EGF-CT was reported in our previous study.[17] To study the interactions between mBAG-1-UBH and proHB-EGF-CT mutants, the ITC experiments were performed with proHB-EGF-CT-R188E and proHB-EGF-CT-ΔH208 (the deletion of His^{208}). The protein and peptide samples were dissolved in 20 mM PBS buffer (pH 6.0) containing 100 mM NaCl. All experiments were performed at 25 °C using a VP-ITC calorimeter (MicroCal). The calorimetry cell containing 1.4 mL of 0.08 mM mBAG-1-UBH was titrated with 240 μL of 1.5 mM proHB-EGF-CT-R188E or proHB-EGF-CT-ΔH208. The titration curve was analyzed using Origin version 7.0 (OriginLab).

Determination of the Binary Complex Structure of proHB-EGF-CT and mBAG-1-UBH. On the basis of the molecular docking method, the solution structure of proHB-EGF-CT in complex form was first calculated using distance geometry followed by simulated annealing techniques. The NOE cross-peaks were automatically assigned, and the peak intensities were iteratively converted to inter proton distance restraints using ARIA.[30] The NOE assignments given in the first ARIA round were checked manually, and the unambiguous and ambiguous NOE restraints derived from the ARIA outputs were further analyzed and employed as inputs for the next round of calculations. In total, 75 distance restraints were collected for the calculation of the structure of proHB-EGF-CT in a complex state; 200 structures were calculated using ARIA and were further refined in explicit solvent using CNS.[31] From this process, an ensemble of the 10 best structures with the lowest energies was obtained. The complex structure of proHB-EGF-CT bound to mBAG-1-UBH was further calculated using HADDOCK (high-ambiguity-driven docking) in combination with CNS.[31−33] The Protein Data Bank (PDB) coordinates of mBAG-1-UBH were obtained from our previous work (PDB entry 2LWP). The residues that showed chemical shift perturbations in the ^{1}H−^{15}N HSQC spectra were used to define the ambiguous interaction restraints (AIRs). Two sets of CSPs were conducted for determination of the structure of the protein−protein complex: one was taken from ^{15}N-labeled proHB-EGF-CT titrated with unlabeled mBAG-1-UBH to obtain the CSP on the proHB-EGF-CT part, and the second was derived using a reversed strategy to find the CSP on the mBAG-1-UBH part (previously reported[17]). NACCESS was employed to identify the solvent-exposed residues in both proHB-EGF-CT and mBAG-1-UBH. In addition, four intermolecular NOEs obtained from ^{13}C F1-filtered, F3-edited NOESY-HSQC experiments were also utilized for structure docking. All upper limit distances for intermolecular NOEs were set to 6 Å. A total of 5000 structures were calculated in a HADDOCK run. The proHB-EGF-CT/mBAG-1-UBH complex structures were clustered and sorted on the basis of the HADDOCK score. The 20 lowest-energy structures derived from the top-ranked HADDOCK cluster were selected for water refinement and further analysis.

RESULTS AND DISCUSSION

NMR Solution Structure of proHB-EGF-CT in Complex Form. Almost complete assignment of ^{1}H, ^{13}C, and ^{15}N resonances of binding of proHB-EGF-CT to unlabeled mBAG-1-UBH was achieved using standard procedures (described in Materials and Methods). On the basis of the chemical shifts of HN, Hα, Cα, Cβ, CO, and N, the TALOS+ prediction[34] reveals that no secondary structure (α-helix or β-sheet) was observed within the 24-amino acid peptide proHB-EGF-CT (data not shown). The three-dimensional NMR structure of proHB-EGF-CT in complex form was determined by using 75 NOE distance restraints. Panels C and D of Figure 1 show an ensemble of the 10 best structures of proHB-EGF-CT in complex form and its ribbon representation of the average structure. The predominant folded conformation of proHB-EGF-CT in solution is mainly constrained by six long-range NOEs (Table 1). The distance restraints from approximately residue 7 to close to the end (residue ∼21), Asn^{206}−Gly^{190}, −Gly^{191}, and −Gly^{193} and Met^{204}−Gly^{193} in Figure 2A, bring two sites closer to a neck shape and cause the residues between these two sites (amino acids 194−203) to form a turn. With

dx.doi.org/10.1021/bi5003019 | Biochemistry 2014, 53, 1935−1946

Table 1. Structural Statistics of proHB-EGF-CT in Its mBAG-1-UBH-Bound Form

no. of distance restraints	
total	75
intraresidue	42
sequential	23
medium-range	4
long-range	6
constraint violation	
minimal NOE violation (Å)	0.31
maximal NOE violation (Å)	0.64
rmsd for 10 structures, backbone in the whole protein (Å)	1.44
Ramachandran plot (%)	
residues in the most favored region	42.1
residues in additionally allowed regions	52.6
residues in generously allowed regions	0.0
residues in disallowed regions	5.3

regard to other distance restraints, one group (Leu^{202}−Asn^{206} and −Tyr^{192} in Figure 2B,C) limits the flexibility of the turn, and another (Tyr^{186}−Val^{194} in Figure 2C) slightly limits the orientation of the N-terminus. Specifically, these intramolecular NOEs make up and limit the partial peptide folding. The proHB-EGF-CT peptide folds like a random coil with end-to-end contact. Table 1 shows a summary of structural statistics for the bound form of proHB-EGF-CT. The root-mean-square deviation (rmsd) for the backbone atoms in the whole peptide of the 10 best structures was estimated to be 1.44 Å. The Ramachandran plot analysis shows that 42.1% of the residues are in the most favored region, 52.6% in the additionally allowed region, 0% in the generously allowed region, and 5.3% in the disallowed regions. The poor quality shown in the Ramachandran plot was due to a lack of dihedral angle restraints for the structure determination, because 20 residues (of 24) in proHB-EGF-CT were predicted to be "dynamic" residues by TALOS+ chemical shift analysis (data not shown).

As shown in the sequence in Figure 1B, proHB-EGF-CT contains three clusters of charged residues, corresponding to the basic residues in the N-terminus (first cluster), the acidic residues in the middle (second cluster), and the basic residues in the C-terminus (third cluster). The precursor forms of five known EGF family ligands, HB-EGF, TGFα, amphiregulin, betacellulin, and epiregulin, share similar patterns of charged amino acid clusters. Nearly the same three clusters exist in proHB-EGF-CT and pro-amphiregulin-CT. The basic amino acid-rich C-terminus, which is the major binding site for mBAG-1-UBH (discussed below), is identical in the cytoplasmic tail of five EGF ligands. Considering the arrangement of the charged residues in the sequence, together with the orientation of peptide folding in the solution structure of proHB-EGF-CT, which reveals two regions with positively charged potential divided by the negatively charged region (Figure 1E,F), we reclassify the three clusters of charged residues. The first cluster includes Arg^{185}, His^{187}−Arg^{189}, and His^{208}. The second cluster includes Asp^{193}, Glu^{195}, Glu^{197}, and Glu^{198}, and the third cluster includes Lys^{199} and Lys^{201}. Our data suggest that the charge−charge interactions may play an important role in binding of proHB-EGF-CT to mBAG-1-UBH.

Binding Site Mapping of mBAG-1-UBH on proHB-EGF-CT by NMR Titration. The chemical shift perturbations of ^{15}N−^{1}H HSQC cross-peaks induced upon addition of mBAG-1-UBH provide useful information for identifying the potential mBAG-1-UBH binding site on the proHB-EGF-CT peptide. Figure 3A shows the ^{15}N−^{1}H HSQC spectra of proHB-EGF-CT in the absence and presence of mBAG-1-UBH at a 1:1 molar ratio. Interaction of mBAG-1-UBH results in significant chemical shift changes of the following resonances at the two termini of proHB-EGF-CT: His^{187}−Gly^{190} and His^{208} (Figure 3B). All of these residues except Gly^{190} are basic amino acids. The structural fold of the proHB-EGF-CT peptide indicates that the contacts between residues 191−193 and 202−206 allow the perturbed residues to come together to form a HRRH-like motif (His^{187}Arg^{188}Arg^{189} close to His^{208}), as shown in Figure 3C. Considering the electrostatic potential on the proHB-EGF-CT surface, the HRRH-like motif forms a positively charged binding pocket for the interaction of mBAG-1-UBH (Figure 3D).

Solution Structure of the proHB-EGF-CT/mBAG-1-UBH Complex. To identify the molecular features of the proHB-EGF-CT/mBAG-1-UBH complex, the three-dimensional structure of the complex was determined by an NMR-based protein docking algorithm. PDB coordinates, including the solution structure of the proHB-EGF-CT peptide calculated in complex form (Figure 1D) and the mBAG-1-UBH structure determined previously (PDB entry 2LWP),[17] were utilized to perform the molecular docking studies. The reason for using the free mBAG-1-UBH structure, which comprises two α-helices (α1 and α2) and five antiparallel β-strands in a β1−β2−α1−α2−β3−β4−β5 topology, was that only small chemical shift perturbations were induced upon titration of proHB-EGF-CT, implying that the binding interaction does not lead a significant structural change in mBAG-1-UBH. Figure 4A shows the superimposition of the backbone atoms of the 20 energy-minimized structures with an rmsd of 0.54 Å representing the structure of the proHB-EGF-CT/mBAG-1-UBH complex, revealing a good agreement among applied CSP restraints for HADDOCK calculations. The proHB-EGF-CT/mBAG-1-UBH binary complex coordinates and NMR restraints have been deposited in the PDB as entry 2M8S. There are 11 residues in mBAG-1-UBH and six residues in proHB-EGF-CT involved in the binding interface with an area of 279.6 Å^2. The regions at the two termini of proHB-EGF-CT interact with those at the C-terminal loop after β-strand β5 and the turn/loop between β-strands β1 and β2 of mBAG-1-UBH (Figure 4B). Residues employed as "active" residues in the HADDOCK calculation and found to be consistent with the interface residues on proHB-EGF-CT and mBAG-1-UBH are colored cyan and pink in the inset of Figure 4B, respectively. However, residues Ile^{92} and Thr^{23} of mBAG-1-UBH, which are defined as the "active" residues on the basis of the results from NMR titration experiments and solvent accessibility analysis, are not involved in the direct binding but are close to the complex interface. This phenomenon is most likely due to the slight change in the chemical environment neighboring the binding site. In addition, four intermolecular NOEs serve as the unambiguous restraints in defining the distances of interacting atoms to be <5 Å (Figure 4C), including Glu^{94} H$_\gamma$ to His^{187} H$_\alpha$, Glu^{94} H$_\gamma$ to Arg^{188} H$_\beta$, Asn^{26} H$_\beta$ to His^{208} H$_\alpha$, and Asn^{26} H$_\beta$ to His^{208} H$_\beta$ between mBAG-1-UBH and proHB-EGF-CT. Figure 4D shows the assignments of intermolecular NOEs based on analysis of the correlation between the ^{1}H chemical shifts of ^{15}N- and ^{13}C-labeled mBAG-1-UBH (X-axis) and unlabeled proHB-EGF-CT (Y-axis) found in the ^{13}C F1-filtered, F3-edited NOESY-HSQC spectra. The interactions observed from

dx.doi.org/10.1021/bi5003019 | Biochemistry 2014, 53, 1935−1946

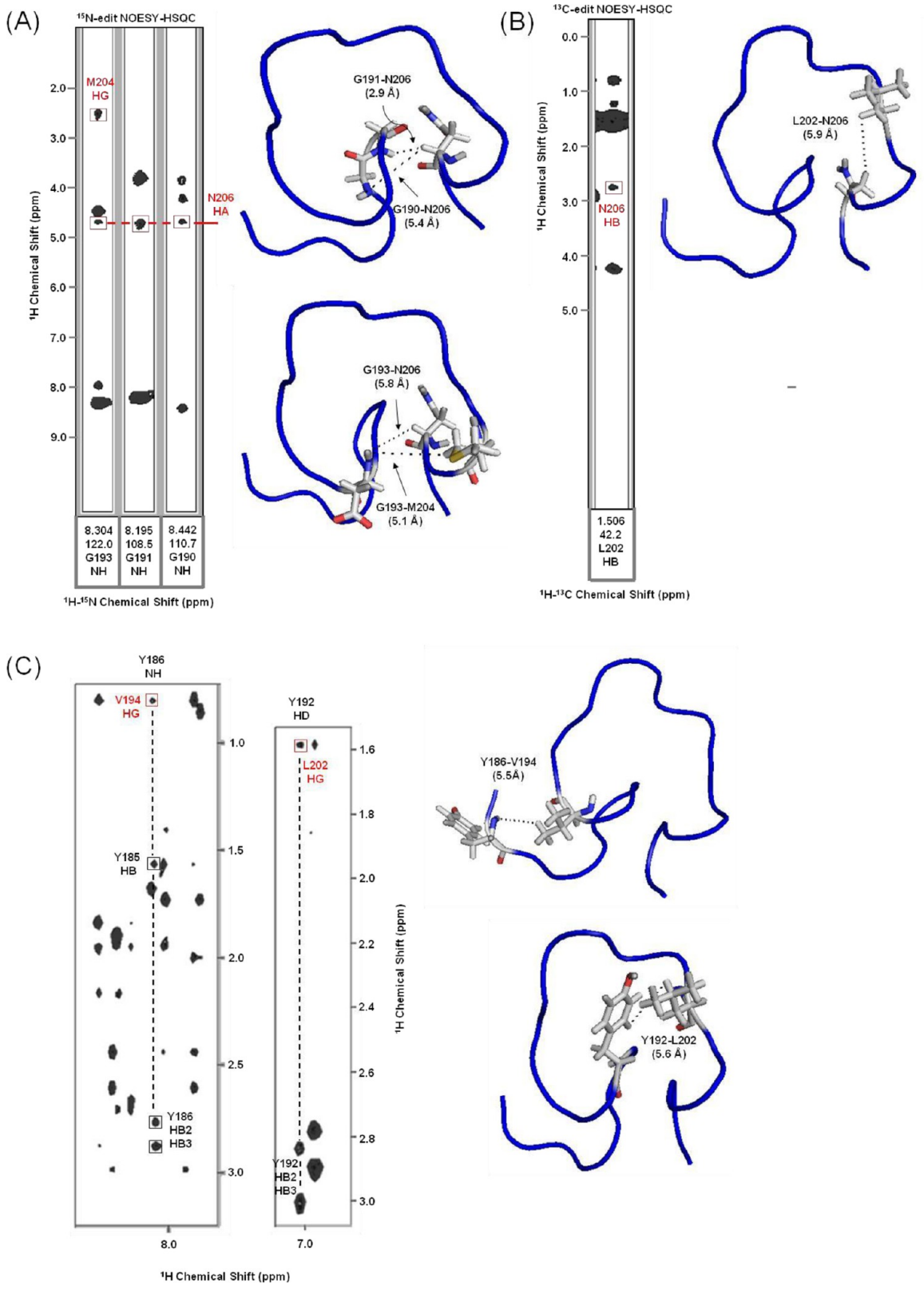

Figure 2. Intramolecular NOEs essential for the overall structural fold of proHB-EGF-CT. (A) Strip plots of the three-dimensional (3D) ^{15}N-edited NOESY-HSQC, (B) 3D ^{13}C-edited NOESY-HSQC, and (C) 2D ^{1}H−^{1}H NOESY spectra showing the NOE cross-peaks between residue atoms. The cross-peaks corresponding to the essential NOEs are boxed in red and labeled with residue pairs on the structure of proHB-EGF-CT on the right side of each panel. There are six long-range intramolecular NOEs and one medium-range intramolecular NOE that have been assigned, including Gly^{191}–Asn^{206}, Gly^{190}–Asn^{206}, Gly^{193}–Asn^{206}, Gly^{193}–Met^{204}, Tyr^{186}–Val^{194}, Tyr^{192}–Leu^{202}, and Leu^{202}–Asn^{206} NOEs.

Glu^{94} (mBAG-1-UBH) to His^{187}/Arg^{188} (proHB-EGF-CT) and from Asn^{26} (mBAG-1-UBH) to His^{208} (proHB-EGF-CT) suggest that the mBAG-1-UBH/proHB-EGF-CT complex could be driven by the charge−charge interactions.

dx.doi.org/10.1021/bi5003019 | *Biochemistry* 2014, 53, 1935−1946

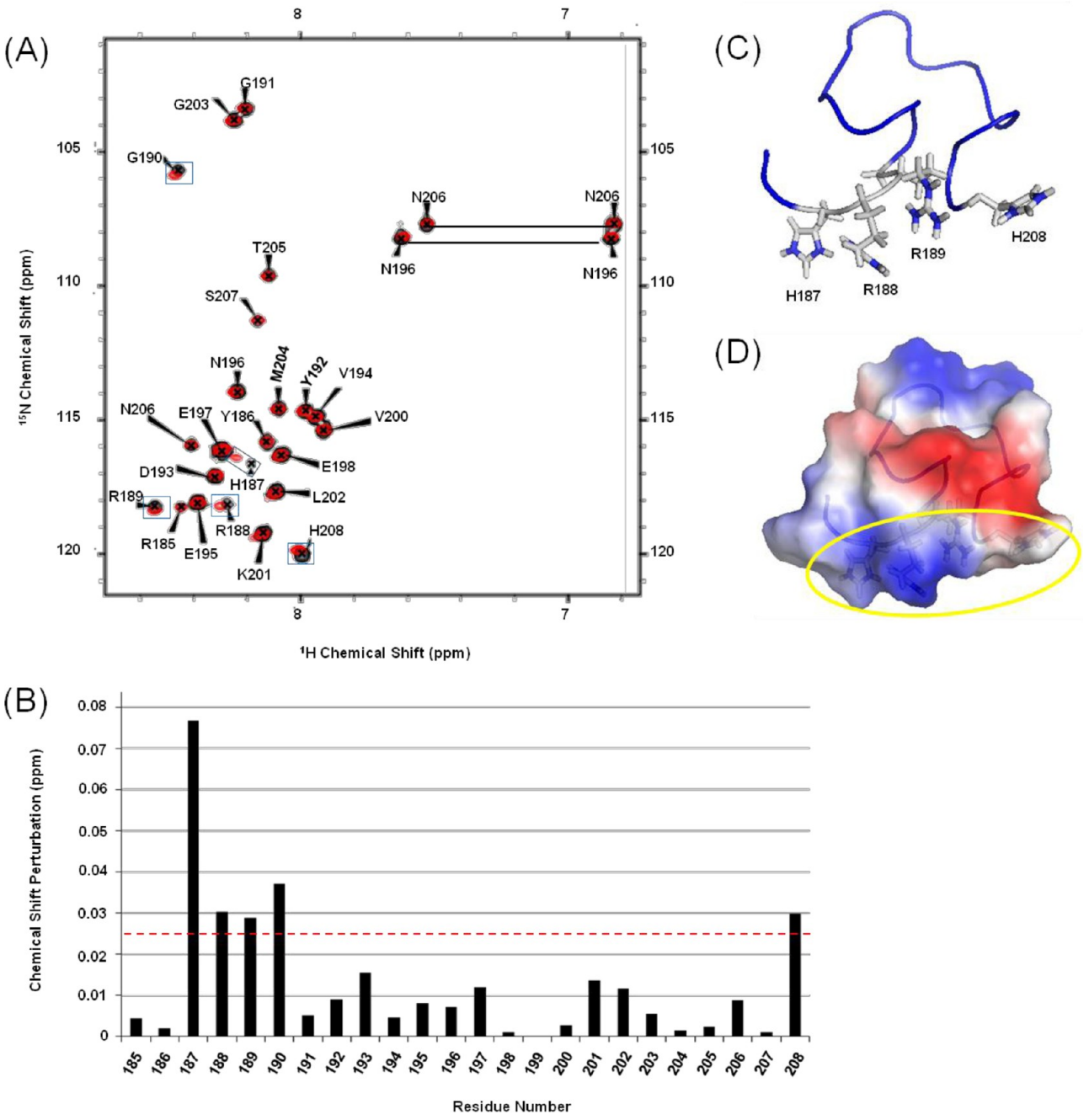

Figure 3. Mapping of the chemical shift-perturbed residues on the solution structure of proHB-EGF-CT upon titration of mBAG-1-UBH. (A) Overlaid 2D ^{1}H−^{15}N HSQC spectra highlight the differences between free proHB-EGF-CT (black) and mBAG-1-UBH-bound proHB-EGF-CT (red). (B) Weighted average of the ^{15}N and ^{1}H chemical shift perturbations $[(0.04\delta_N^2 + \delta_H^2)^{0.5}]$ of residues in proHB-EGF-CT induced by formation of the complex with mBAG-1-UBH. The dashed line is intended to indicate the residues exhibiting significant chemical shift perturbations (>0.025 ppm). Residues with the most significant chemical shift perturbations, including His^{187}, Arg^{188}, Arg^{189}, Gly^{190}, and His^{208}, are boxed in blue in panel A. (C) The residues affected by mBAG-1-UBH binding are labeled and shown as white stick side chains on the NMR structure of proHB-EGF-CT. (D) Semitransparent electrostatic potential surface of proHB-EGF-CT showing the residues involved in binding. The corresponding mBAG-1-UBH binding region is shown in the yellow oval.

As described above (see NMR Solution Structure of proHB-EGF-CT in Complex Form), the composition of charged residues contributes to a highly charged surface for the proHB-EGF-CT peptide, which has been classified into three regions on the basis of the electrostatic potential. A negatively charged region is sandwiched between two positively charged regions (Figure 1F). In the mBAG-1-UBH protein, analysis of the surface electrostatic potential indicates that one side of the protein surface is mainly negatively charged and the opposite side is relatively positively charged. In the mBAG-1-UBH/proHB-EGF-CT complex, one of the positively charged regions on the proHB-EGF-CT peptide binds to the mainly negatively charged region on the mBAG-1-UBH protein (Figure 4E). The insights gathered from the electrostatic potential analysis of both proteins also confirm that the charge−charge interactions could be the dominant force driving the binding event between mBAG-1-UBH and proHB-EGF-CT.

dx.doi.org/10.1021/bi5003019 | *Biochemistry* 2014, 53, 1935−1946

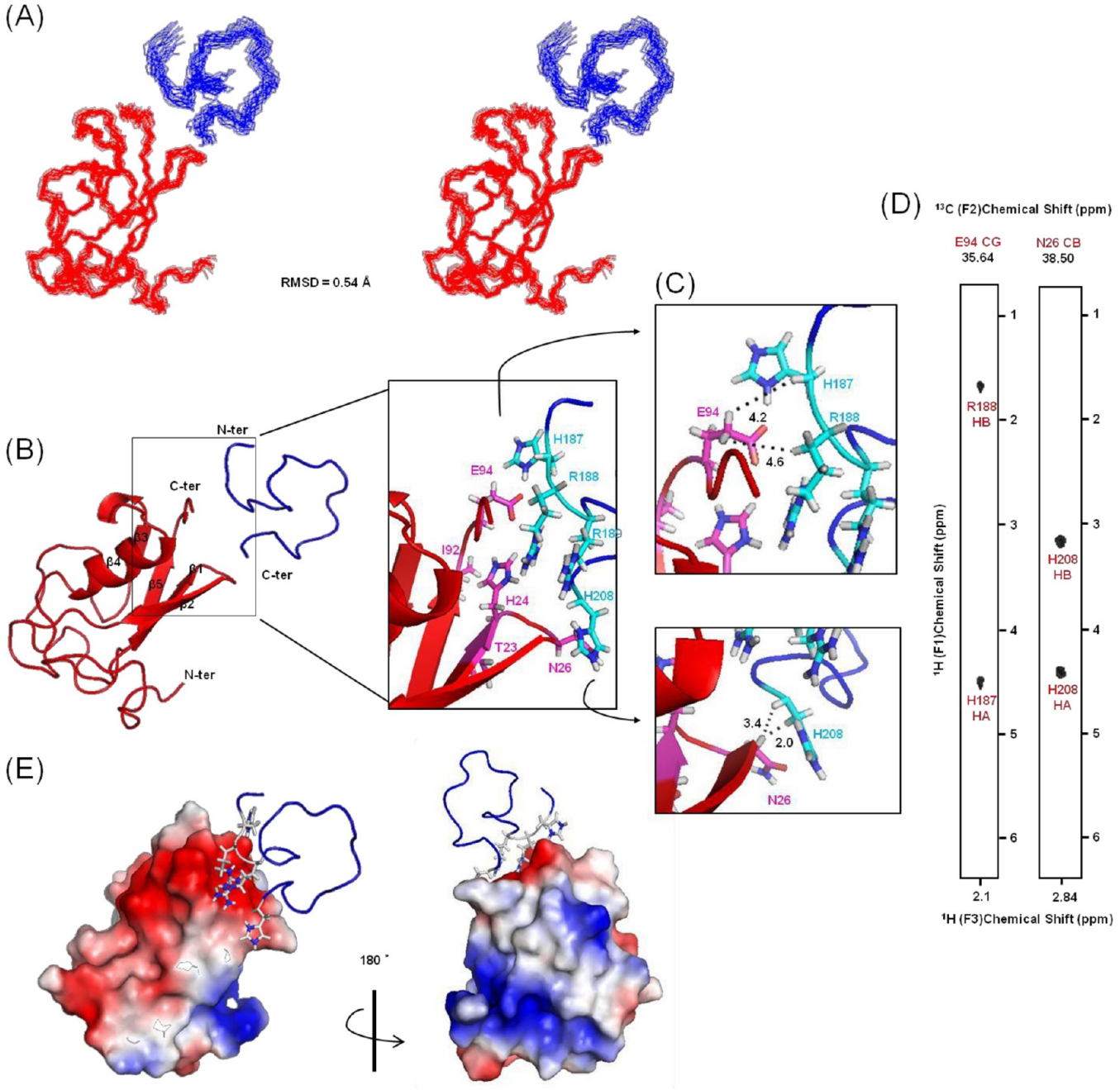

Figure 4. Solution structure of the proHB-EGF-CT/mBAG-1-UBH binary complex and identification of residues contributing to the binding interface. (A) Superposition of the 20 final solution structures of the proHB-EGF-CT/mBAG-1-UBH binary complex with a stereo backbone representation. proHB-EGF-CT is colored blue and mBAG-1-UBH red. (B) Ribbon representation of the binary complex and the magnified diagram of the binding interface. The inset shows the side chains of the perturbed residues derived from NMR mapping experiments on both mBAG-1-UBH (labeled in pink) and proHB-EGF-CT (labeled in cyan). (C) The intermolecular NOEs used for the identification of the protein−peptide interface are indicated by the dashed line with the distance given in angstroms. (D) Strip plots of the three-dimensional ^{13}C F1-filtered, F3-edited NOESY-HSQC spectra showing the intermolecular NOEs between unlabeled proHB-EGF-CT (with signals observed in the ^{1}H F1 dimension) and ^{15}N- and ^{13}C-labeled mBAG-1-UBH (with signals observed in ^{13}C F2 and ^{1}H F1 dimensions). (E) View (180°) of the binary complex shown as a semitransparent electrostatic potential surface in mBAG-1-UBH and a ribbon representation with stick side chains (interacting residues) in proHB-EGF-CT.

Molecular Interactions between proHB-EGF-CT and mBAG-1-UBH Confirmed by the proHB-EGF-CT Mutants. In our previous work,[17] the proHB-EGF-CT binding affinity of mBAG-1-UBH was estimated to be 6.9 μM with a negative enthalpy change (ΔH = −1.97 kcal/mol) and a positive entropy change (ΔS = 17.0 cal mol^{-1} deg^{-1}) by using isothermal titration calorimetry, implying that the binding could be driven by the enthalpy contribution through hydrogen bond formation, electrostatic interaction, or van der Waals force. In combination with the HSQC titration data, electrostatic interactions could be the dominant forces for the formation of the mBAG-1-UBH/proHB-EGF-CT complex. To further confirm the observation, we used ITC to investigate the interactions of the mBAG-1-UBH protein with two proHB-

dx.doi.org/10.1021/bi5003019 | *Biochemistry* 2014, 53, 1935−1946

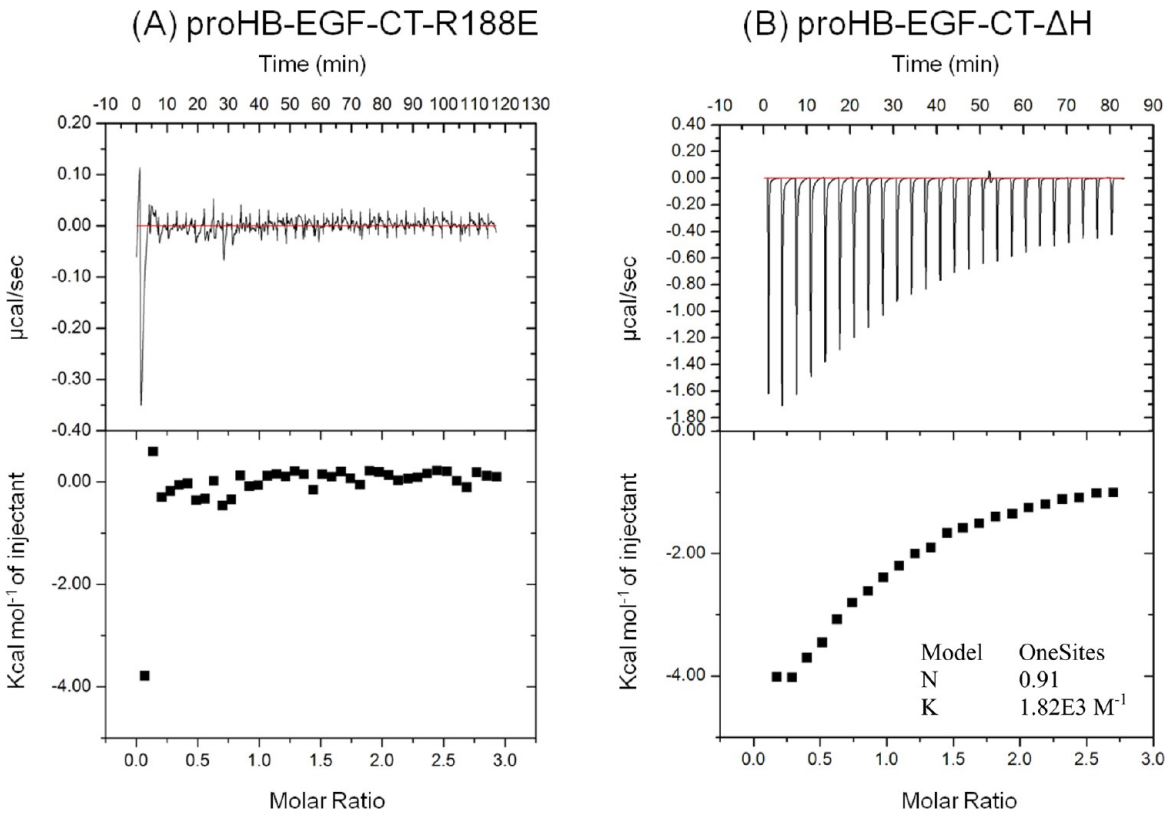

Figure 5. Binding affinity measurements for the proHB-EGF-CT-R188E and proHB-EGF-CT-ΔH208 mutants with mBAG-1-UBH using ITC. Representative ITC profiles of (A) proHB-EGF-CT-R188E and (B) proHB-EGF-CT-ΔH208 titrated with mBAG-1-UBH. The raw data of the titrations are shown in the top panels, and the integrated data obtained after subtracting the heat of dilution are shown in the bottom panels for each experiment. The titration curve fitting to a one-site binding model indicates an equilibrium dissociation constant (K_d) of 0.55 mM for the interaction between proHB-EGF-CT-R188E and mBAG-1-UBH. All the experiments were performed using a VP-ITC calorimeter (MicroCal) at 25 °C. The calorimeter cell containing 1.4 mL of 0.08 mM mBAG-1-UBH was titrated by the injection of 240 μL of 1.5 mM proHB-EGF-CT-R188E and proHB-EGF-CT-ΔH208. All the proteins were prepared in a buffer of 20 mM PBS (pH 6.0) containing 100 mM NaCl.

EGF-CT mutants, including proHB-EGF-CT-R188E and proHB-EGF-CT-ΔH208. These two mutants were designed on the basis of the binding interface within the determined proHB-EGF-CT/mBAG-1-UBH complex structure. Three residues at the N-terminus (His^{187}, Arg^{188}, and Arg^{189}) and one residue at the C-terminus (His^{208}) of proHB-EGF-CT have been considered as the crucial residues binding to mBAG-1-UBH (Figure 4B). To corroborate the contribution of charge−charge interactions, we decided to mutate one of the basic residues at the N-terminus to an acidic amino acid, because the opposite charge may produce a repulsion effect interfering with the electrostatic interactions between proHB-EGF-CT and mBAG-1-UBH, and constructed the mutant proHB-EGF-CT-R188E. On the other hand, the C-terminal residue His^{208} of proHB-EGF-CT was directly truncated to eliminate its interaction with Asn^{26} of mBAG-1-UBH. Figure 5A shows the ITC profile of mBAG-1-UBH titrated with the mutant proHB-EGF-CT-R188E. The result reveals that no heat change was detected during titration, suggesting that mutation of residue Arg^{188} of proHB-EGF-CT completely abolished the interaction with mBAG-1-UBH. In comparison, similar to the observation with the wild-type peptide, an exothermic reaction curve was also observed after titration of the mBAG-1-UBH protein with the proHB-EGF-CT-ΔH208 peptide (Figure 5B). However, the titration curve fitting to a one-site binding model reveals a 1:1 stoichiometry with an equilibrium dissociation constant (K_d) of 0.55 mM for the proHB-EGF-CT-ΔH208/mBAG-1-UBH interaction, indicating that truncation of residue His^{208} results in an 80-fold weaker affinity than the binding of wild-type proHB-EGF-CT to the mBAG-1-UBH protein. These results suggest that the charged residues at the N- and C-termini of proHB-EGF-CT are necessary for its binding to mBAG-1-UBH, confirming that the electrostatic interactions are indeed responsible for the formation of the complex. Interestingly, the N-terminal mutation (R188E) totally inhibits the binding of proHB-EGF-CT to mBAG-1-UBH, whereas the C-terminal truncation (ΔH208) only weakens the binding affinity. These results imply that residues at the N-terminus comprise the major binding region on proHB-EGF-CT and the C-terminal basic residue might further facilitate the formation of the complex with mBAG-1-UBH. In addition, the *in vivo* importance of interaction sites on proHB-EGF-CT was confirmed by Lin et al., revealing that in the presence of BAG-1 the deletion of the proHB-EGF C-terminal tail results in cell apoptosis.[11]

Backbone Dynamic Studies of proHB-EGF-CT and the proHB-EGF-CT/mBAG-1-UBH Complex. To further understand the molecular interactions of proHB-EGF-CT with mBAG-1-UBH, we investigated the backbone motions of proHB-EGF-CT in the absence and presence of mBAG-1-UBH at a 1:1 molar ratio by measuring ^{15}N R_1 and R_2 relaxation rates and ^{1}H−^{15}N steady-state heteronuclear NOEs (Figure 6A−C). When mBAG-1-UBH binds, our data show that only residues located at or near the region of the binding site on proHB-

dx.doi.org/10.1021/bi5003019 | *Biochemistry* 2014, 53, 1935−1946

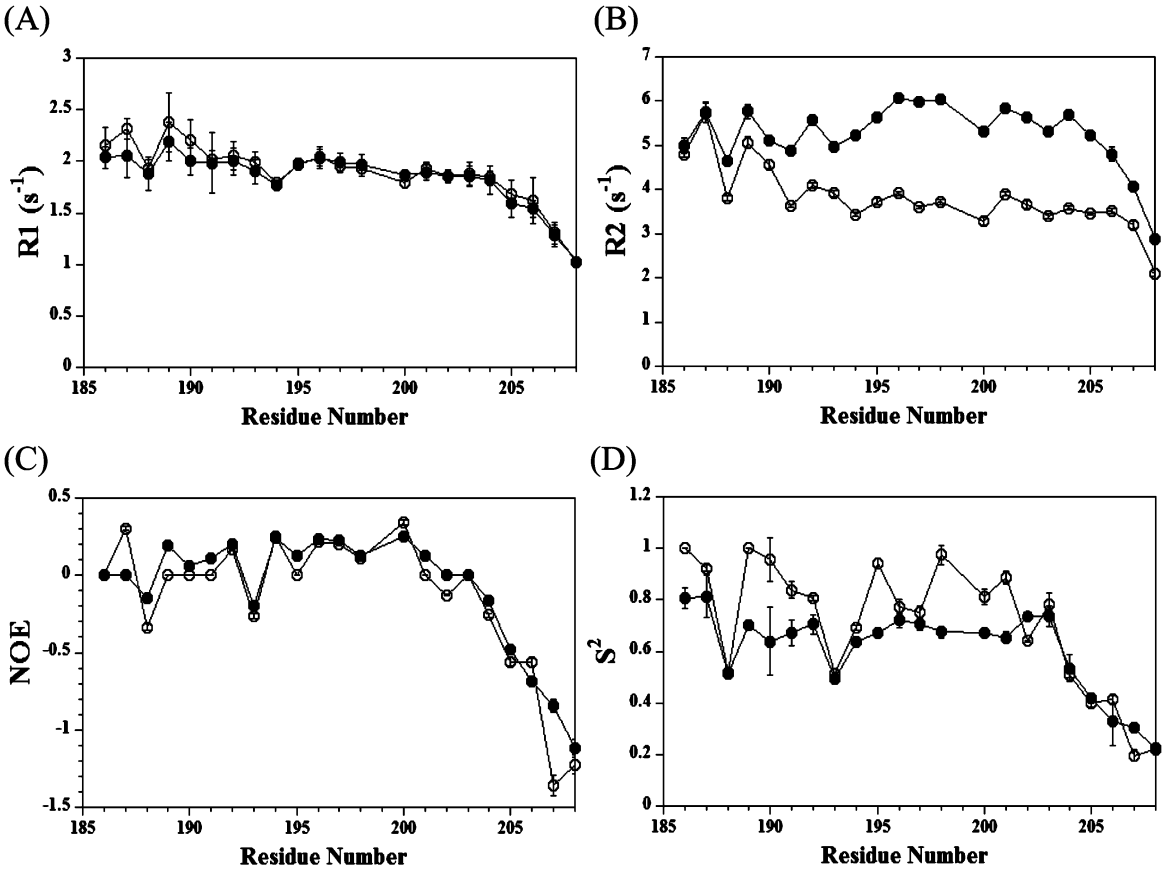

Figure 6. Relaxation parameters of proHB-EGF-CT alone (●) and in complex with mBAG-1-UBH (○). The values of (A) ^{15}N R_1 relaxation rates, (B) ^{15}N R_2 relaxation rates, (C) ^{1}H−^{15}N steady-state heteronuclear NOEs, and (D) S^2 order parameters are shown as a function of residue number in the proHB-EGF-CT sequence. All experimental data were acquired at 700 MHz and 25 °C.

EGF-CT experience larger changes in R_1 and NOE values (including Tyr^{186}, His^{187}, Arg^{189}, and Gly^{190} for R_1 and His^{187} and Asn^{207} for NOE), while most residues reveal significant decreases in R_2 values (except Tyr^{186} and His^{187}). Interestingly, both the proHB-EGF-CT proteins in free form and in complex with mBAG-1-UBH possess low or negative NOE values, indicating a high degree of structural flexibility. To confirm these observations, a ModelFree approach was utilized for the further studies. The results indicate that additional parameters (R_{ex}) are required to fit all residues in proHB-EGF-CT without or with mBAG-1-UBH (data not shown). Figure 6D shows order parameters S^2 extracted from the primary relaxation data and reveals that mBAG-1-UBH interactions result in the obviously increased S^2 values of residues Tyr^{186}, His^{187}, Arg^{189}, Gly^{190}, Gly^{191}, Glu^{195}, Glu^{198}, Val^{200}, and Lys^{201}. These data confirm the importance of proHB-EGF-CT N-terminal residues for interactions and indicate that mBAG-1-UBH binding mainly contributes to reduce the extent of conformational exchange motion of proHB-EGF-CT, with the average R_{ex} decreasing from 2.64 to 1.33 Hz.

Structural Insight into the Multifunctional Peptide, proHB-EGF-CT. The 24-amino acid cytoplasmic tail of proHB-EGF shows a high degree of sequence conservation across species (95% identical mouse and human amino acid sequences), suggesting a potential functional role for this peptide segment. Several biological activities of the proHB-EGF-CT peptide have been reported in recent studies on the basis of the identification of important residues. Figure 7 shows the mapping of regions responsible for various functions onto

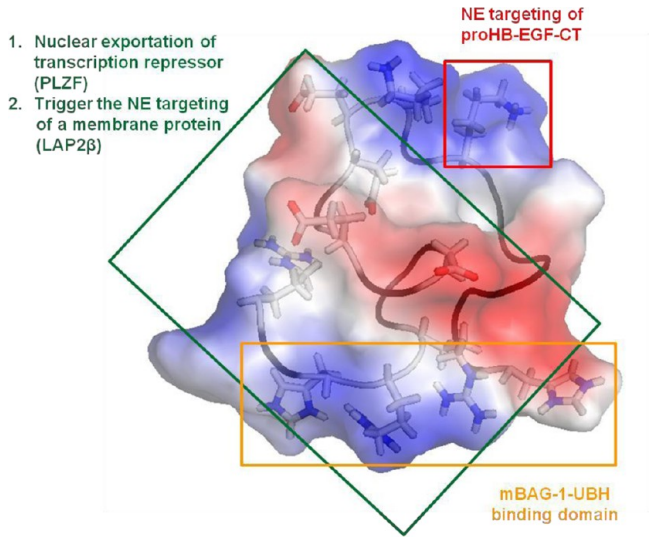

Figure 7. Functional motifs of the proHB-EGF-CT peptide. Various residue groups with reported functions are mapped and illustrated on the solution structure of proHB-EGF-CT shown as a semitransparent electrostatic potential surface with the stick side chains of interacting residues.

the solution structure of proHB-EGF-CT. The green-boxed region, corresponding to the first and second clusters defined in the solution structure of proHB-EGF-CT in complex form, is correlated to the interaction with the transcription repressor,

dx.doi.org/10.1021/bi5003019 | *Biochemistry* 2014, 53, 1935−1946

PLZF, leading to its nuclear exportation[10] and the ability to trigger the nuclear envelope (NE) targeting of a membrane protein.[16] However, the individual significance of the first and second clusters has not been characterized so far for NE trafficking. The red-boxed residue Lys[201] shown in Figure 7, located in the third cluster in the proHB-EGF-CT peptide, is essential for the NE targeting of proHB-EGF-CT itself.[16] The yellow box indicates the region in the proHB-EGF-CT peptide, the first cluster, responsible for the mBAG-1-UBH interactions presented in this study. Our finding reveals that each cluster in the proHB-EGF-CT peptide exhibits a specific binding target for the biological functions related to cellular protein trafficking. Interestingly, the mBAG-1-UBH binding region on the proHB-EGF-CT peptide (first cluster region) is also involved in the region responsible for NE targeting, supporting the hypothesis that proHB-EGF-CT is most likely able to trigger the nuclear translocation of BAG-1 in keeping its level high.

Possible Molecular Mechanism Underlying the Synergistic Anti-apoptosis Activity of proHB-EGF-CT and mBAG-1-UBH. So far, several studies have revealed the critical role of nuclear BAG-1 in the cell survival function.[15,35−37] For instance, cellular stress triggers the translocation of the cytoplasmic BAG-1S isoform to the nucleus.[36] Interestingly, a similar phenomenon was also observed for proHB-EGF-CT after a shedding stimulus.[15] One possible explanation is that the two proteins cooperate in the nuclear targeting pathway. Although the sequence of proHB-EGF-CT is not conserved with the classical NLS, the pattern of two clusters of basic amino acids separated by a spacer of a few amino acids is similar.[38] On the basis of the results of this study, we propose a model to explain the molecular mechanism underlying the anti-apoptosis activity mediated by the interactions of proHB-EGF-CT and mBAG-1-UBH. One possible mechanism is one in which the 24-amino acid peptide, proHB-EGF-CT, serves as a unique nonclassical NLS to trigger the nuclear translocation of BAG-1S. The crucial binding motif on the peptide is mainly composed of basic amino acids, which is the same as in the classical NLS. Subsequently, BAG-1 is able to bind to nuclear hormone receptors (such as ER) and inhibit cell apoptosis.[39,40] This is the first study in which the BAG-1 interaction sites on proHB-EGF-CT have been characterized. However, the mechanism proposed for the anti-apoptosis activity needs to be further validated with more detailed studies characterizing the nuclear targeting pathway.

■ CONCLUSIONS

Previous research has focused on the functional significance of binding of proHB-EGF-CT to mBAG-1-UBH, and the NMR structure described here complements the molecular interactions within the protein/peptide system. On the basis of reported studies, it is possible that the synergistic effect of two proteins on the anti-apoptosis activity may be mediated by proHB-EGF triggering the nuclear translocation of mBAG-1. The mechanism by which nuclear-localized BAG-1 may protect against apoptosis remains to be elucidated. In this study, the three-dimensional NMR solution structure of the proHB-EGF-CT peptide complexed with the mBAG-1-UBH protein allows for the identification of the residues in both the protein and the peptide involved in molecular interactions. Our results reveal the key binding site residues and suggest that charge−charge interactions are the predominant force involved in the binding. Furthermore, the NMR solution structure of the conserved 24-residue proHB-EGF-CT peptide exhibits three clusters that can be distinguished on the basis of their distinct surface electrostatic potentials. The reported functional residues were also mapped onto the structure of the multifunctional peptide, indicating that various cellular protein trafficking-related functions are mediated by distinct regions on the proHB-EGF-CT peptide. This is the first report of the structure of the proHB-EGF-CT peptide, which provides valuable information for the design of future experimental and modeling studies for understanding the detailed mechanism of protein trafficking. Moreover, further effort is needed to characterize the cytoplasmic domains of other EGF family precursors.

■ AUTHOR INFORMATION

Corresponding Authors

*Department of Chemistry, National Tsing Hua University, Hsinchu 30013, Taiwan. Fax: 886-3-5711082. Telephone: 886-3-5721524. E-mail: cyu.nthu@gmail.com.

*Instrumentation Center, National Tsing Hua University, Hsinchu 30013, Taiwan. Fax: 886-3-5711082. Telephone: 886-3-5715131, ext. 35605. E-mail: kuowei@mx.nthu.edu.tw.

Funding

This work was supported by grants from the National Science Council of the Republic of China (NSC 100-2113-M-007-012-MY3 to C.Y. and NSC 102-2731-M-007-002-MY2 to K.-W.H.).

Notes

The authors declare no competing financial interest.

■ ACKNOWLEDGMENTS

We gratefully acknowledge the use of the Varian NMR 700 MHz spectrometer at the Instrumentation Center of National Tsing Hua University supported by the NSC of Taiwan.

■ ABBREVIATIONS

HB-EGF, heparin binding EGF-like growth factor; BAG-1, Bcl-2-associated athanogene 1; NMR, nuclear magnetic resonance; HSQC, heteronuclear single-quantum coherence spectroscopy; CSP, chemical shift perturbation; ITC, isothermal titration calorimetry; NOESY, nuclear Overhauser enhancement spectroscopy; ARIA, ambiguous restraints for iterative assignment; CNS, crystallography and NMR system; HADDOCK, high-ambiguity-driven docking.

■ REFERENCES

(1) Higashiyama, S., Abraham, J., Miller, J., Fiddes, J., and Klagsbrun, M. (1991) A heparin-binding growth factor secreted by macrophage-like cells that is related to EGF. *Science 251*, 936−939.

(2) Hieda, M., Isokane, M., Koizumi, M., Higashi, C., Tachibana, T., Shudou, M., Taguchi, T., Hieda, Y., and Higashiyama, S. (2008) Membrane-anchored growth factor, HB-EGF, on the cell surface targeted to the inner nuclear membrane. *J. Cell Biol. 180*, 763−769.

(3) Goishi, K., Higashiyama, S., Klagsbrun, M., Nakano, N., Umata, T., Ishikawa, M., Mekada, E., and Taniguchi, N. (1995) Phorbol ester induces the rapid processing of cell surface heparin-binding EGF-like growth factor: Conversion from juxtacrine to paracrine growth factor activity. *Mol. Biol. Cell 6*, 967−980.

(4) Dethlefsen, S. M., Raab, G., Moses, M. A., Adam, R. M., Klagsbrun, M., and Freeman, M. R. (1998) Extracellular calcium influx stimulates metalloproteinase cleavage and secretion of heparin-binding EGF-like growth factor independently of protein kinase C. *J. Cell. Biochem. 69*, 143−153.

(5) Takenobu, H., Yamazaki, A., Hirata, M., Umata, T., and Mekada, E. (2003) The Stress- and Inflammatory Cytokine-induced Ectodomain Shedding of Heparin-binding Epidermal Growth Factor-like Growth Factor Is Mediated by p38 MAPK, Distinct from the 12-O-

Tetradecanoylphorbol-13-acetate- and Lysophosphatidic Acid-induced Signaling Cascades. *J. Biol. Chem. 278*, 17255−17262.
(6) Chalaris, A., Rabe, B., Paliga, K., Lange, H., Laskay, T., Fielding, C. A., Jones, S. A., Rose-John, S., and Scheller, J. (2007) Apoptosis is a natural stimulus of IL6R shedding and contributes to the proinflammatory trans-signaling function of neutrophils. *Blood 110*, 1748−1755.
(7) Steinhusen, U., Weiske, J., Badock, V., Tauber, R., Bommert, K., and Huber, O. (2001) Cleavage and Shedding of E-cadherin after Induction of Apoptosis. *J. Biol. Chem. 276*, 4972−4980.
(8) Shimura, T., Yoshida, M., Fukuda, S., Ebi, M., Hirata, Y., Mizoshita, T., Tanida, S., Kataoka, H., Kamiya, T., Higashiyama, S., and Joh, T. (2012) Nuclear translocation of the cytoplasmic domain of HB-EGF induces gastric cancer invasion. *BMC Cancer 12*, 205.
(9) Kinugasa, Y., Hieda, M., Hori, M., and Higashiyama, S. (2007) The Carboxyl-terminal Fragment of Pro-HB-EGF Reverses Bcl6-mediated Gene Repression. *J. Biol. Chem. 282*, 14797−14806.
(10) Nanba, D., Toki, F., and Higashiyama, S. (2004) Roles of charged amino acid residues in the cytoplasmic domain of proHB-EGF. *Biochem. Biophys. Res. Commun. 320*, 376−382.
(11) Lin, J., Hutchinson, L., Gaston, S. M., Raab, G., and Freeman, M. R. (2001) BAG-1 Is a Novel Cytoplasmic Binding Partner of the Membrane Form of Heparin-binding EGF-like Growth Factor. *J. Biol. Chem. 276*, 30127−30132.
(12) Hirata, Y., Ogasawara, N., Sasaki, M., Mizushima, T., Shimura, T., Mizoshita, T., Mori, Y., Kubota, E., Wada, T., and Tanida, S. (2009) BCL6 degradation caused by the interaction with the C-terminus of pro-HB-EGF induces cyclin D2 expression in gastric cancers. *Br. J. Cancer 100*, 1320−1329.
(13) Nanba, D., Mammoto, A., Hashimoto, K., and Higashiyama, S. (2003) Proteolytic release of the carboxy-terminal fragment of proHB-EGF causes nuclear export of PLZF. *J. Cell Biol. 163*, 489−502.
(14) Townsend, P. A., Cutress, R. I., Sharp, A., Brimmell, M., and Packham, G. (2003) BAG-1: A multifunctional regulator of cell growth and survival. *Biochim. Biophys. Acta 1603*, 83−98.
(15) Barnes, J. D., Arhel, N. J., Lee, S. S., Sharp, A., Al-Okail, M., Packham, G., Hague, A., Paraskeva, C., and Williams, A. C. (2005) Nuclear BAG-1 expression inhibits apoptosis in colorectal adenoma-derived epithelial cells. *Apoptosis 10*, 301−311.
(16) Hieda, M., Isokane, M., Koizumi, M., Higashi, C., Tachibana, T., Shudou, M., Taguchi, T., Hieda, Y., and Higashiyama, S. (2008) Membrane-anchored growth factor, HB-EGF, on the cell surface targeted to the inner nuclear membrane. *J. Cell Biol. 180*, 763−769.
(17) Huang, H.-W., and Yu, C. (2013) The NMR solution structure of the ubiquitin homology domain of Bcl-2-associated athanogene 1 (BAG-1-UBH) from *Mus musculus*. *Biochem. Biophys. Res. Commun. 431*, 86−91.
(18) Huang, H.-W., and Yu, C. (2012) Backbone and side-chain resonance assignments (^{1}H, ^{15}N and ^{13}C) of the ubiquitin homology domain of mouse BAG-1. *Biomol. NMR Assignments*, 1−5.
(19) Ikura, M., Kay, L. E., and Bax, A. (1990) A novel approach for sequential assignment of proton, carbon-13, and nitrogen-15 spectra of larger proteins: Heteronuclear triple-resonance three-dimensional NMR spectroscopy. Application to calmodulin. *Biochemistry 29*, 4659−4667.
(20) Bax, A., and Ikura, M. (1991) An efficient 3D NMR technique for correlating the proton and^{15}N backbone amide resonances with the α-carbon of the preceding residue in uniformly^{15}N/^{13}C enriched proteins. *J. Biomol. NMR 1*, 99−104.
(21) Muhandiram, D. R., and Kay, L. E. (1994) Gradient-Enhanced Triple-Resonance Three-Dimensional NMR Experiments with Improved Sensitivity. *J. Magn. Reson., Ser. B 103*, 203−216.
(22) Grzesiek, S., Anglister, J., and Bax, A. (1993) Correlation of Backbone Amide and Aliphatic Side-Chain Resonances in ^{13}C/^{15}N-Enriched Proteins by Isotropic Mixing of ^{13}C Magnetization. *J.Magn. Reson., Ser. B 101*, 114−119.
(23) Grzesiek, S., and Bax, A. (1993) Amino acid type determination in the sequential assignment procedure of uniformly ^{13}C/^{15}N-enriched proteins. *J. Biomol. NMR 3*, 185−204.
(24) Bax, A., Clore, G. M., and Gronenborn, A. M. (1990) ^{1}H^{1}H correlation via isotropic mixing of ^{13}C magnetization, a new three-dimensional approach for assigning ^{1}H and ^{13}C spectra of ^{13}C-enriched proteins. *J. Magn. Reson. 88*, 425−431.
(25) Marion, D., Driscoll, P. C., Kay, L. E., Wingfield, P. T., Bax, A., Gronenborn, A. M., and Clore, G. M. (1989) Overcoming the overlap problem in the assignment of proton NMR spectra of larger proteins by use of three-dimensional heteronuclear proton-nitrogen-15 Hartmann-Hahn-multiple quantum coherence and nuclear Overhauser-multiple quantum coherence spectroscopy: Application to interleukin 1β. *Biochemistry 28*, 6150−6156.
(26) Kumar, A., Ernst, R. R., and Wüthrich, K. (1980) A two-dimensional nuclear Overhauser enhancement (2D NOE) experiment for the elucidation of complete proton-proton cross-relaxation networks in biological macromolecules. *Biochem. Biophys. Res. Commun. 95*, 1−6.
(27) Lee, W., Revington, M. J., Arrowsmith, C., and Kay, L. E. (1994) A pulsed field gradient isotope-filtered 3D ^{13}C HMQC-NOESY experiment for extracting intermolecular NOE contacts in molecular complexes. *FEBS Lett. 350*, 87−90.
(28) Goddard, T. D., and Kneller, D. G. (2008) *SPARKY 3*, University of California, San Francisco.
(29) Yagi, H., Ishimoto, K., Hiromoto, T., Fujita, H., Mizushima, T., Uekusa, Y., Yagi-Utsumi, M., Kurimoto, E., Noda, M., Uchiyama, S., Tokunaga, F., Iwai, K., and Kato, K. (2012) A non-canonical UBA-UBL interaction forms the linear-ubiquitin-chain assembly complex. *EMBO Rep. 13*, 462−468.
(30) Rieping, W., Habeck, M., Bardiaux, B., Bernard, A., Malliavin, T. E., and Nilges, M. (2007) ARIA2: Automated NOE assignment and data integration in NMR structure calculation. *Bioinformatics 23*, 381−382.
(31) Brünger, A. T., Adams, P. D., Clore, G. M., DeLano, W. L., Gros, P., Grosse-Kunstleve, R. W., Jiang, J. S., Kuszewski, J., Nilges, M., Pannu, N. S., Read, R. J., Rice, L. M., Simonson, T., and Warren, G. L. (1998) Crystallography & NMR System: A New Software Suite for Macromolecular Structure Determination. *Acta Crystallogr. D54*, 905−921.
(32) de Vries, S. J., van Dijk, A. D. J., Krzeminski, M., van Dijk, M., Thureau, A., Hsu, V., Wassenaar, T., and Bonvin, A. M. J. J. (2007) HADDOCK versus HADDOCK: New features and performance of HADDOCK2.0 on the CAPRI targets. *Proteins: Struct., Funct., Bioinf. 69*, 726−733.
(33) Dominguez, C., Boelens, R., and Bonvin, A. M. J. J. (2003) HADDOCK: A Protein−Protein Docking Approach Based on Biochemical or Biophysical Information. *J. Am. Chem. Soc. 125*, 1731−1737.
(34) Shen, Y., Delaglio, F., Cornilescu, G., and Bax, A. (2009) TALOS+: A hybrid method for predicting protein backbone torsion angles from NMR chemical shifts. *J. Biomol. NMR 44*, 213−223.
(35) Noguchi, T., Takeno, S., Shibata, T., Fumoto, S., Uchida, Y., Yokoyama, S., Gabbert, H. E., and Müller, W. (2003) Nuclear BAG-1 expression is a biomarker of poor prognosis in esophageal squamous cell carcinoma. *Diseases of the Esophagus 16*, 107−111.
(36) Townsend, P. A., Cutress, R. I., Sharp, A., Brimmell, M., and Packham, G. (2003) BAG-1 Prevents Stress-induced Long-term Growth Inhibition in Breast Cancer Cells via a Chaperone-dependent Pathway. *Cancer Res. 63*, 4150−4157.
(37) Yamauchi, H., Adachi, M., Sakata, K.-i., Hareyama, M., Satoh, M., Himi, T., Takayama, S., Reed, J. C., and Imai, K. (2001) Nuclear BAG-1 localization and the risk of recurrence after radiation therapy in laryngeal carcinomas. *Cancer Lett. 165*, 103−110.
(38) Dingwall, C., Robbins, J., Dilworth, S. M., Roberts, B., and Richardson, W. D. (1988) The nucleoplasmin nuclear location sequence is larger and more complex than that of SV-40 large T antigen. *J. Cell Biol. 107*, 841−849.
(39) Zeiner, M., and Gehring, U. (1995) A protein that interacts with members of the nuclear hormone receptor family: Identification and cDNA cloning. *Proc. Natl. Acad. Sci. U.S.A. 92*, 11465−11469.

(40) Kullmann, M., Schneikert, J., Moll, J., Heck, S., Zeiner, M., Gehring, U., and Cato, A. C. B. (1998) RAP46 Is a Negative Regulator of Glucocorticoid Receptor Action and Hormone-induced Apoptosis. *J. Biol. Chem.* 273, 14620−14625.